Author Manuscript

Author Manuscript

Author Manuscript

Author Manuscript

HHS Public Access

Author manuscript

Nano Lett. Author manuscript; available in PMC 2023 June 19.

Published in final edited form as:

Nano Lett. 2021 May 26; 21(10): 4255–4261. doi:10.1021/acs.nanolett.1c00405.

Multi-mode Time-resolved Superresolution Microscopy Revealing Chain Packing and Anisotropic Single Carrier Transport in Conjugated Polymer Nanowires

Yifei Jiang[‡], **Haobin Chen**[‡,§], **Xiaoju Men**[£], **Zezhou Sun**[§], **Zhen Yuan**[£], **Xuanjun Zhang**[£], **Daniel T. Chiu**[‡], **Changfeng Wu**[§], **Jason McNeill**[†]

[†]Department of Chemistry, Clemson University, Clemson, South Carolina 29634, United States

[‡]Department of Chemistry, University of Washington, Seattle, Washington 98195, United States

[§]Department of Biomedical Engineering, Southern University of Science and Technology, Shenzhen, Guangdong 518055, China

[£]Faculty of Health Science, University of Macau, Taipa 999078, Macau

Abstract

Here, we developed a novel, multi-mode superresolution method to perform full-scale structural mapping and measure the energy landscape for single carrier transport along conjugated polymer nanowires. Through quenching of the local emission, the motion of a single photo-generated hole was tracked using blinking-assisted localization microscopy. Then, utilizing binding and unbinding dynamics of quenchers onto the nanowires, local emission spectra were collected sequentially and assembled to create a superresolution map of emission sites throughout the structure. The hole polaron trajectories were overlaid with the superresolution maps to correlate structures with charge transport properties. Using this method, we compared the efficiency of inter- and intra-chain hole transport inside the nanowires and for the first time directly measured the depth of carrier traps originated from torsional disorder and chemical defects.

Graphical Abstract

Corresponding Authors: Jason McNeill - Department of Chemistry, Clemson University, Clemson, South Carolina 29634, United States; mcneill@clemson.edu, Changfeng Wu - Department of Biomedical Engineering, Southern University of Science and Technology, Shenzhen, Guangdong 518055, China; wucf@sustc.edu.cn, Yifei Jiang - Department of Chemistry, University of Washington, Seattle, Washington 98195, United States; yifeij@uw.edu.

The authors declare no competing financial interest.

ASSOCIATED CONTENT

Supporting Information

Experimental procedures and methods, synthesis of do-PFO polymer, evolution of morphology, determination of localization uncertainties, recognizing quenching/recovery steps, analysis of hole polaron hopping dynamics resolved by the two methods, modulation of single nanowire emission by excitation polarization, change transport parameter distributions.

Author Manuscript Author Manuscript Author Manuscript Author Manuscript

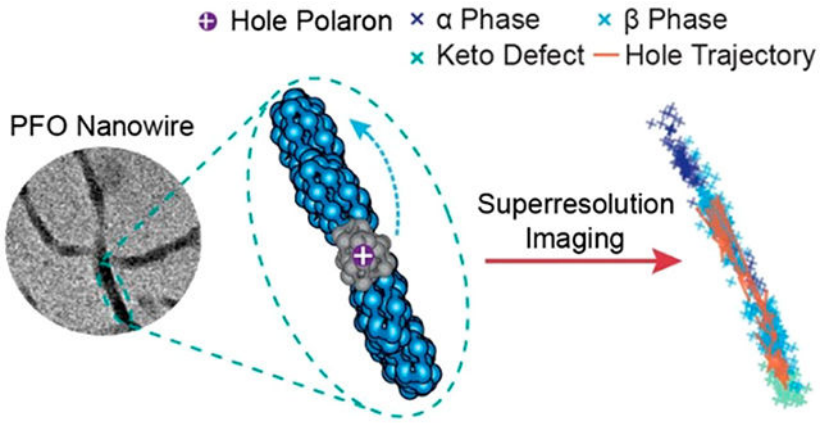

Keywords

charge transport; conjugated polymer nanowire; fluorescence quenching; nanostructure; superresolution microscopy

Conjugated polymers exhibit many degrees of conformational freedom and weak inter-chain interactions, which result in complex structure at nanoscale.[1–3] The heterogeneous structure leads to dispersive charge transport behavior and limits the performance of conjugated polymer based devices.[3–5] Recent research has shown that well-controlled anisotropic conjugated polymer nanostructures, such as nanorods and nanowires, exhibit increased charge carrier mobility and improved performance for a variety of applications.[6–9] Investigation of charge transport dynamics in these systems could help us establish a clearer relationship between nanostructure and charge transport properties. However, previous studies of charge transport in conjugated polymer nanostructure typically combine electron microscopy with ensemble voltage-current analysis, which involves averaging over large areas and many charge carriers.[6, 10] As such, important information about local structure, such as inter- and intra-chain coupling strength, the physical nature (spatial extent, depth) of charge carrier trap sites, and how these parameters dictate single carrier transport remains unclear. Obtaining a deeper understanding about the nanostructure-charge transport property relationship is crucial for the continued development of conjugated polymer based devices.

Recently, single-molecule/superresolution microscopy has emerged as promising tools for characterization of conjugated oligomer/polymer nanostructure as well as charge transport dynamics.[11–18] However, as single molecule approaches, these methods depend critically on photon budget, which limits the amount of obtainable information. There is currently a lack of method that can characterize single carrier dynamics with high spatial/temporal resolution, while providing complete structural information. In this work, we overcome these limitations by developing a novel, tracking and hyperspectral imaging approach, which first tracks nanoscale hole polaron motion at 1 kHz framerate, then utilizes binding and unbinding dynamics of water-soluble quenchers onto the nanostructure to reconstruct superresolution map of emission sites throughout the structure. By overlaying the hole polaron trajectories with the superresolution maps, structural information can be correlated with charge transport properties.

Author Manuscript Author Manuscript Author Manuscript Author Manuscript

We used this method to characterize charge transport in poly(9,9-dioctylfluorene) (PFO) nanowires. The nanowire emission showed strong dependence on excitation polarization, indicating extended chain-packing along the longitudinal axis. Tracking of single photo-generated holes in the pristine nanowires revealed that hole polarons exhibited efficient anisotropic transport through the β phase, yielding intra-chain and inter-chain zero-field hole mobilities of 10^{-7}-10^{-6} cm^2/Vs and 10^{-9}-10^{-7} cm^2/Vs, respectively. A variety of 0–0/0–1 peak ratios were observed in the local β phase emission spectra. It was found that the inter-chain hole mobilities decreased with increasing of the 0–0/0–1 emission peak ratio, whereas the intra-chain hole mobilities showed an opposite trend, indicating that the anisotropic charge transport was strongly dictated by the local intra- and inter-chain coupling strengths.[19–20] The efficiency of long-range hole transport was limited by the presence of the glassy α phase that polaron trapping at the grain boundaries can be observed, which reduced the hole mobilities to 10^{-9}-10^{-8} cm^2/Vs. To investigate the impact of chemical defects on charge transport, the nanowire suspension was excited with a UV lamp in air to induce formation of keto defects. The partially oxidized nanowires exhibited hole mobilities of 10^{-10}-10^{-9} cm^2/Vs, which were two to three orders of magnitude lower than that of the pristine ones. Hole polaron trajectory analysis showed that holes were highly trapped around the chemical defects. From the escape dynamics of hole polaron trapped by the α phase and the keto defects, we estimated the depth of charge carrier traps originated from torsional disorder and chemical defects to be 220–260 meV and 280–340 meV, respectively. These results provided an unprecedented level of detail about anisotropic charge transport at single carrier level and greatly improved our understanding about structure-charge transport property relationship in conjugated polymer nanowires and related systems.

PFO nanowires were synthesized using a novel self-assembly method. In a typical nanoprecipitation process, a solution of conjugated polymer in tetrahydrofuran was rapidly mixed with water under sonication, yielding exclusively spherical nanoparticles.[21–24] We discovered that nanoprecipitation of PFO with side-chain oxetane terminus (do-PFO, Figure S1, synthesis procedures are provided in SI), under the presence of 0.25 wt% Triton X-100, resulted in self-assembly of a variety of nanostructures (Figure 1, Figure S2, S3). The self-assembled nanowires were immobilized on a glass coverslip, and excited with a 405 nm laser, under N_2 atmosphere. For polaron tracking, fluorescence microscopy images were collected using a sCMOS camera, at 1 kHz framerate. Similar to many other conjugated polymer nanostructures, the nanowires exhibited pronounced fluorescence blinking under photoexcitation (Figure 2a, Figure S4), due to temporary oxidation of the conjugated polymers (formation of hole radicals).[25–26] The hole acts as an exciton annihilation center and effectively quenches local emission (see SI for additional discussion). [16, 27–28] There are many excited state processes in conjugated polymers that can generate holes, including photo-induced charge transfer to trace amount of oxygen molecules in the environment, charge transfer to substrate, charge separation at grain boundary, etc.[29–30] The photo-generated holes are typically highly trapped, due to attraction of the opposite charge, self-trapping caused by geometric relaxation of the surroundings, as well as energetic barriers induced by disorder of the material. Highly confined motion with low carrier mobility was previous observed for photo- and electrode-injected holes. [17, 27] In self-assembled

Author Manuscript Author Manuscript Author Manuscript Author Manuscript

PFO nanowires, we observed surprisingly efficient long range hole transport under zero electric field, likely facilitated by the highly ordered β phase. [31] As shown in Figure 2 b–f, a photo-generated hole resulted in a dark spot on the nanowire, which moved along the wire over time. To locate the exact position of the hole polaron, we adapted a frame-by-frame subtraction method that is previously developed for blinking-assisted localization microscopy.[32–33] For nanowire segments that exhibited two-state photo-blinking (Figure 2a), the point-spread-functions (PSFs) during the fluorescence "off" states were subtracted frame-by-frame from the PSF of the adjacent fluorescence "on" state to recover the quenched PSFs (Figure 2b–f), which were then fitted to a 2D Gaussian function to obtain the position of the hole polaron. The localization error of this method is dictated by the localization photon number and shot noise of background fluorophores in the images, respectively.[33] Based on the typical polaron quenching depth and nanowire brightness, the tracking uncertainty at 1 kHz is expected to be 5.6–11.1 nm, which can be further reduced to <5 nm through binning. (Figure S5, see SI for additional discussion).

After polaron tracking, the nanowires were submerged under quencher solution to perform superresolution spectral mapping. We tested various type of water-soluble quenchers, including multiple variants of black hole quenchers and viologen derivatives, and found that methyl-viologen dichloride performed the best for our experiment. Photobleaching-assisted mapping is also possible. [14, 34] However, the formation of emissive keto defects during the photobleaching process could complicate analysis. To obtain spectrum information, a transmission grating was placed in front of the camera to disperse single particle emission. Fluorescence microscopy images were collected at 50 Hz framerate. As methyl-viologen cations (MV^{2+}) adsorbed onto the nanowire, the conjugated polymer emission was gradually quenched due to formation of conjugated polymer/MV^{2+} charge-transfer complex. [35–37] Occasional fluorescence recovery can be observed when a quencher unbound from the surface. A combination of change point analysis and hidden-Markov modeling were used to identify single quenching/recovery steps (Figure 2g, Figure S6–S8, see SI for additional discussion).[38–39] Bleaching/blinking-assisted localization analysis was performed with the single-step quenching and recovery dynamics, i.e., the positions and spectra of the emitters quenched or recovered at each step were determined from the zeroth and the first-order fluorescence spots, respectively. The superresolution images were then overlaid with diffraction-limited images and hole polaron trajectories (Figure 2h, fluorescent beads were used as fiduciary markers for alignment.). As discussed above, the localization error of bleaching/blinking-assisted localization microscopy is determined by the localization photon number and shot noise induced by the background fluorophores. Decreasing of the nanowire intensity resulted in reduced shot noise in the subtracted image and improved localization precision. Typically, as the nanowire emission changes from maximum to fully quenched, the localization error decreases from 5.2–9.0 nm to 2.7–3.6 nm (Figure S5, see SI for additional discussion). However, the actual mapping resolution is defined by the quenching radius of the charge-transfer complex, which was reported to be 5–15 nm, depending on the systems.[40–41] From our tests, 5–10 adsorption events can readily quench the emission from self-assembled ~20 nm PFO beads, which indicates that while the adsorption occurred at the interface, the actual quenched volume was much larger, due to efficient migration of excitons to the electron-deficiencies. We also performed structural mapping using

Author Manuscript Author Manuscript Author Manuscript Author Manuscript

spontaneous polaron motion. As the polaron moves in the nanostructure, different areas are quenched, which allows simultaneous polaron tracking and superresolution mapping through single particle localization and correlated spectrum analysis.[18] The structural information obtained from this method is very limited, as it depended on the random walk of a single carrier. In addition, to ensure enough photons for simultaneous polaron tracking and spectral analysis, the experimental framerate is limited to 50 Hz. Comparison of experiment results obtained from the two methods showed that, while there is consistency in the slower interfacial hopping dynamics resolved, some faster polaron motion was not captured at the 50 Hz frame rate (Figure S9, see SI for additional discussions).

For pristine PFO nanowires, superresolution mapping revealed distinct regions of the α and β phases (Figure 2g, Figure 3a). We found that the β phase was mainly responsible for hole transport in the nanowires. Hole polarons showed rapid oscillation within the β phase and abrupt hopping between the β phases separated by regions characterized by torsional disorder (Figure 3a–d). The nanowire emission showed strong dependence on excitation polarization (Figure S10), indicating extended chain-packing along the longitudinal axis. Mean square displacement (MSD) analysis of polaron motion along and across the nanowires revealed highly anisotropic charge transport. The longitudinal MSD showed two-step behavior with steep increase at the early time and slower increase at longer timescales (Figure 3e), which is consistent with the physical picture of rapid hole transport within the β phase domains and slower inter-domain hopping. Compared to the longitudinal MSD, the transverse MSD showed slower increase with a lower plateau, consistent with slower transverse motion confined by the width of a nanowire (Figure 3e). Both longitudinal and transverse MSD can be fitted to a bi-exponential confined diffusion function. Early time MSD fitting yielded longitudinal and transverse hole mobilities of 10^{-7}-10^{-6} cm^2/Vs and 10^{-9}-10^{-7} cm^2/Vs, respectively (Figure S11). Considering the chain-packing inside the nanowire, these results likely suggested that, within the β phase, the intra-chain hole transport was over one order of magnitude more efficient than the inter-chain hole transport. From the early time confinement length, we estimated the typical domain size of the β phase to be 500–2000 nm^2 (Figure S11). At longer timescale, both the transverse and the longitudinal hole mobilities dropped to 10^{-9}-10^{-8} cm^2/Vs, due to the presence of the glassy α phase. For PFO nanowires with distinct domains of the α and the β phases, we investigated local charge transport behavior by dividing the hole polaron trajectory into small segments and overlaying them with the superresolution map. MSD analysis was performed on the segments for which the hole transport occurred within a single phase. It was observed that the longitudinal hole mobilities within the β phase were almost two orders of magnitude higher than the mobilities within the α phases (Figure S11). From the local β phase emission spectra, we observed a variety of 0–0/0–1 emission peak ratios (Figure 3c). The intra- and inter-chain hole mobilities determined from the early time MSD showed dependence on the local spectra. As shown in Figure 3f, the inter-chain hole mobilities decreased with increasing of the 0–0/0–1 emission peak ratio, whereas the intra-chain hole mobilities showed an opposite trend. These results are consistent with the previous research, which showed that the 0–0/0–1 peak ratio indicated the competition between intra- and inter-chain couplings in conjugated polymer systems. [19–20] For conjugated polymer structures with strong intra-chain coupling, emission from the lowest edge of the excited state vibronic

Author Manuscript Author Manuscript Author Manuscript Author Manuscript

bands is strongly allowed that the 0–0 peak typically has the highest intensity. In contrast, for conjugated polymer structures with strong inter-chain coupling, the 0–0 transition has low oscillator strength and the side band transitions become dominant, which results in lower 0–0/0–1 peak intensity ratio.

As discussed earlier, the presence of torsional disorder limited the long-range charge transport efficiency in the nanowires. Besides disorder, long-term operation and exposure to molecular oxygen can induce formation of chemical defects in PFO devices, which can also reduce charge carrier mobility. [42–44] To compare the impact of structural disorder and chemical defects on charge transport, polaron tracking was also performed with partially oxidized PFO nanowires. The nanowire suspension was excited with a UV lamp in air to induce formation of keto defects. Superresolution mapping of the partially oxidized nanowires showed distinct areas with broadband green emission, consistent with the spectral signature of fluorenone. [42–43] Hole polarons generated in the photo-oxidized nanowires exhibited complex motion occurring on multiple timescales. Trapping by both chemical defects and disorder can be observed for the same hole polaron (Figure 4a). To separate the two kinds of trapping dynamics, we divided hole polaron trajectories into small segments and analyzed them using MSD. In some segments, we observed that the hole polarons were highly confined within the β phase and exhibited trapping/release dynamics near the grain boundaries (figure 4b–e), whereas in some other segments, hole polarons were found to be highly trapped around the chemical defects, i.e., slow transitions between the fluorenone and a few local sites can be observed (Figure 4f–i). The two kinds of trapping dynamics yielded very different MSD. Polarons trapped by chemical defects typically exhibited highly restricted motion with the MSD showing confined diffusion behavior and mobilities ranging from 10^{-10} to 10^{-9} cm^2/Vs (Figure 4j, Figure S11). For polarons showing disorder trapping, the MSD showed two-step behavior similar to that observed for pristine nanowires (Figure 4j). The steep early increase corresponds to confined motion within the β phase, whereas the slower confined diffusion occurring on longer timescales corresponds to interfacial trapping. The mobilities of the interfacial hole polarons were estimated from fitting of the MSD tails, which ranged from 10^{-9} to 10^{-8} cm^2/Vs (Figure 4j). Change point and autocorrelation analysis were performed with the escape dynamics of polaron trapped by the α phase and keto defects (Figure S12, see SI for additional discussion). We found that disorder trapping occurred on millisecond timescale, whereas the average time that a polaron resided in a keto defect was nearly an order of magnitude longer (Figure 4k). By plugging the polaron hopping time and distance into the Miller-Abrahams equation, we estimated the overall energy barrier for disorder and defect trapping to be 370–410 meV and 430–490 meV, respectively. Assuming a polaron binding energy of 150 meV, the actual depths of hole traps originated from torsional disorder and keto defects are 220–260 meV and 280–340 meV, respectively (Figure 4l). [45–46] These results are consistent with previous electro-chemical studies of fluorenone, which showed that the highest occupied molecular orbital (HOMO) of fluorenone is 200–300 meV higher than the HOMO of fluorene,[47] making them hole traps in PFO systems. In contrast, in pristine PFO nanowires, hole polaron likely possesses lower energy within the ordered β phase, through delocalization along the polymer backbone. As a result, hole polarons were highly confined within the β phase and disorder trapping mostly occurred at the grain boundary.

Author Manuscript Author Manuscript Author Manuscript Author Manuscript

In summary, we developed a novel, multi-mode superresolution imaging method to perform full-scale structural mapping and measure the energy landscape for single carriers transport along conjugated polymer nanowires. Through quenching of the local emission, the motion of a single photo-generated hole was tracked using blinking-assisted localization microscopy. Then, utilizes binding and unbinding dynamics of quenchers onto the nanowire, local emission spectra were collected sequentially and assembled to obtain a superresolution map of emission sites throughout the structure. Superresolution mapping revealed that the nanowires exhibited semi-crystalline structures with distinct regions of the α and β phases. In pristine nanowires, it was observed that hole polarons mainly transported through the β phase and were occasionally trapped at the grain boundaries. Rapid anisotropic motion can be observed for polarons within the β phase, yielding intra-chain and inter-chain hole mobilities of 10^{-7}-10^{-6} cm^2/Vs and 10^{-9}-10^{-7} cm^2/Vs, respectively. A variety of 0–0/0–1 peak ratios were observed in the local β phase emission spectra. It was found that the inter-chain hole mobilities decreased with increasing of the 0–0/0–1 emission peak ratio, whereas the intra-chain hole mobilities showed an opposite trend, indicating that the charge transport is strongly dictated by the local intra- and inter-chain coupling strengths. The presences of disorder and chemical defects were found to greatly reduce charge transport efficiency. In partially oxidized nanowires, holes were highly trapped around the keto defects, yielding mobilities of 10^{-10}-10^{-9} cm^2/Vs, whereas mobilities of 10^{-9}-10^{-8} cm^2/Vs were obtained from polarons trapped at the α and β phase grain boundaries. From the escape dynamics of polaron trapped by the α phase and the keto defects, we estimated the depth of the two kinds of hole traps to be 220–260 meV and 280–340 meV, respectively. Overall, the unprecedented sensitivity of our method makes it uniquely suited for characterization of single carrier dynamics on nanoscale and correlating nanostructure with charge transport properties. In comparison, conventional methods for charge transport characterization, such as time-of-fight and I-V analysis, are ensemble measurement involving averaging over large areas and many carriers. [10, 48–49] As a result, the single carrier transport parameters can only be interpreted indirectly through Monte-Carlo simulation and comparison with the experimental results, making it difficult to obtain a clear structure-charge transport property relationship. While we only demonstrated polaron tracking and structural mapping in conjugated polymer nanowires in this work, the method can be readily applied to various other nanoscale conjugated polymer systems as well as nanostructures of other materials, where similar charge carrier induced fluorescence quenching behavior is presented. Characterization of single carrier transport in these nanoscale systems could offer a unique window to such process in bulk materials and provide implications for optimizing semiconductor structures for specific applications.

Supplementary Material

Refer to Web version on PubMed Central for supplementary material.

ACKNOWLEDGEMENTS

JDM acknowledges financial support from the NSF (Grant No. CHE-1412694). CW acknowledges the National Key R&D Program of China (Grant No. 2020YFA0909000, 2018YFB0407200), National Natural Science Foundation of China (Grant No. 81771930) and the Shenzhen Science and Technology Innovation Commission

Author Manuscript Author Manuscript Author Manuscript Author Manuscript

(Grant No. KQTD20170810111314625). DTC acknowledges financial support from the National Institutes of Health (R01MH113333).

REFERENCES

1. Noriega R; Rivnay J; Vandewal K; Koch FP; Stingelin N; Smith P; Toney MF; Salleo A, A general relationship between disorder, aggregation and charge transport in conjugated polymers. Nat. Mater. 2013, 12 (11), 1038–1044. [PubMed: 23913173]
2. Panzer F; Bässler H; Lohwasser R; Thelakkat M; Köhler A, The impact of polydispersity and molecular weight on the order–disorder transition in poly (3-hexylthiophene). J. Phys. Chem. Lett. 2014, 5 (15), 2742–2747. [PubMed: 26277973]
3. Tessler N; Preezant Y; Rappaport N; Roichman Y, Charge transport in disordered organic materials and its relevance to thin-film devices: a tutorial review. Adv. Mater. 2009, 21 (27), 2741–2761.
4. Bässler H; Köhler A, Charge transport in organic semiconductors. In Unimolecular and Supramolecular Electronics I; Metzger RM, Eds; Springer: Verlag Berlin Heidelberg, 2012; pp 1–65.
5. Forrest SR; Thompson ME, Introduction: organic electronics and optoelectronics. Chem. Rev. 2007, 107 (4), 923–925.
6. Dong H; Jiang S; Jiang L; Liu Y; Li H; Hu W; Wang E; Yan S; Wei Z; Xu W, Nanowire crystals of a rigid rod conjugated polymer. J. Am. Chem. Soc. 2009, 131 (47), 17315–17320. [PubMed: 19891486]
7. O'carroll D; Lieberwirth I; Redmond G, Microcavity effects and optically pumped lasing in single conjugated polymer nanowires. Nat. Nanotechnol. 2007, 2 (3), 180–184. [PubMed: 18654250]
8. Lei Y; Li N; Chan W-KE; Ong BS; Zhu F, Highly sensitive near infrared organic phototransistors based on conjugated polymer nanowire networks. Org. Electron. 2017, 48, 12–18.
9. Ren S; Chang L-Y; Lim S-K; Zhao J; Smith M; Zhao N; Bulovic V; Bawendi M; Gradecak S, Inorganic–organic hybrid solar cell: bridging quantum dots to conjugated polymer nanowires. Nano Lett. 2011, 11 (9), 3998–4002. [PubMed: 21859097]
10. Lee MJ; Gupta D; Zhao N; Heeney M; McCulloch I; Sirringhaus H, Anisotropy of charge transport in a uniaxially aligned and chain-extended, high-mobility, conjugated polymer semiconductor. Adv. Funct. Mater. 2011, 21 (5), 932–940.
11. Reznik C; Darugar Q; Wheat A; Fulghum T; Advincula RC; Landes CF, Single ion diffusive transport within a poly (styrene sulfonate) polymer brush matrix probed by fluorescence correlation spectroscopy. J. Phys. Chem. B 2008, 112 (35), 10890–10897. [PubMed: 18630854]
12. So WY; Hong J; Kim JJ; Sherwood GA; Chacon-Madrid K; Werner JH; Shreve AP; Peteanu LA; Wildeman J, Effects of solvent properties on the spectroscopy and dynamics of alkoxy-substituted PPV oligomer aggregates. J. Phys. Chem. B 2012, 116 (35), 10504–10513. [PubMed: 22721432]
13. Kim HJ; Kwon Y; Yang H; Devanny AJ; Kaufman LJ, Spatial and spectral superresolution imaging for characterizing multichromophoric systems. J. Phys. Chem. C 2020, 124 (46), 25568–25577.
14. Park H; Hoang DT; Paeng K; Kaufman LJ, Localizing exciton recombination sites in conformationally distinct single conjugated polymers by super-resolution fluorescence imaging. ACS Nano 2015, 9 (3), 3151–3158. [PubMed: 25743935]
15. Hu Z; Adachi T; Haws R; Shuang B; Ono RJ; Bielawski CW; Landes CF; Rossky PJ; Vanden Bout DA, Excitonic energy migration in conjugated polymers: the critical role of interchain morphology. J. Am. Chem. Soc. 2014, 136 (45), 16023–16031. [PubMed: 25268474]
16. Yu J; Wu C; Tian Z; McNeill J, Tracking of single charge carriers in a conjugated polymer nanoparticle. Nano Lett. 2012, 12 (3), 1300–1306. [PubMed: 22313320]
17. Jiang Y; Nongnual T; Groff L; McNeill J, Nanoscopy of single charge carrier jumps in a conjugated polymer nanoparticle. J. Phys. Chem. C 2018, 122 (2), 1376–1383.
18. Jiang Y; McNeill J, Superresolution mapping of energy landscape for single charge carriers in plastic semiconductors. Nat. Commun. 2018, 9 (1), 4314. [PubMed: 30333490]
19. Spano FC; Silva C, H-and J-aggregate behavior in polymeric semiconductors. Annu. Rev. Phys. Chem. 2014, 65, 477–500. [PubMed: 24423378]

Author Manuscript Author Manuscript Author Manuscript Author Manuscript

20. Niles ET; Roehling JD; Yamagata H; Wise AJ; Spano FC; Moulé AJ; Grey JK, J-aggregate behavior in poly-3-hexylthiophene nanofibers. J. Phys. Chem. Lett. 2012, 3 (2), 259–263.
21. Wu C; Chiu DT, Highly fluorescent semiconducting polymer dots for biology and medicine. Angew. Chem. Int. Ed. 2013, 52 (11), 3086–3109.
22. Jiang Y; Novoa M; Nongnual T; Powell R; Bruce T; McNeill J, Improved superresolution imaging using telegraph noise in organic semiconductor nanoparticles. Nano Lett. 2017, 17 (6), 3896–3901. [PubMed: 28537735]
23. Jiang Y; Hu Q; Chen H; Zhang J; Chiu DT; McNeill JD, Dual-mode superresolution imaging using charge transfer dynamics in semiconducting polymer dots. Angew. Chem. Int. Ed. 2020, 59 (37), 16173–16180.
24. Men X; Yuan Z, Polymer dots for precision photothermal therapy of brain tumors in the second near-infrared window: a mini-review. ACS Appl. Polym. Mater. 2020, 2 (10), 4319–4330.
25. Vanden Bout DA; Yip W-T; Hu D; Fu D-K; Swager TM; Barbara PF, Discrete intensity jumps and intramolecular electronic energy transfer in the spectroscopy of single conjugated polymer molecules. Science 1997, 277 (5329), 1074–1077.
26. Gesquiere AJ; Park S-J; Barbara PF, Hole-induced quenching of triplet and singlet excitons in conjugated polymers. J. Am. Chem. Soc. 2005, 127 (26), 9556–9560. [PubMed: 15984882]
27. Bolinger JC; Traub MC; Adachi T; Barbara PF, Ultralong-range polaron-induced quenching of excitons in isolated conjugated polymers. Science 2011, 331 (6017), 565–567. [PubMed: 21292973]
28. Jiang Y; McNeill J, Light-harvesting and amplified energy transfer in conjugated polymer nanoparticles. Chem. Rev. 2017, 117 (2), 838–859. [PubMed: 28029769]
29. Yu J; Hu D; Barbara PF, Unmasking electronic energy transfer of conjugated polymers by suppression of O_2 quenching. Science 2000, 289 (5483), 1327–1330. [PubMed: 10958774]
30. Reid OG; Pensack RD; Song Y; Scholes GD; Rumbles G, Charge photogeneration in neat conjugated polymers. Chem. Mater. 2013, 26 (1), 561–575.
31. Prins P; Grozema FC; Nehls BS; Farrell T; Scherf U; Siebbeles LD, Enhanced charge-carrier mobility in β-phase polyfluorene. Phys. Rev. B 2006, 74 (11), 113203.
32. Burnette DT; Sengupta P; Dai Y; Lippincott-Schwartz J; Kachar B, Bleaching/blinking assisted localization microscopy for superresolution imaging using standard fluorescent molecules. Proc. Natl. Acad. Sci. U. S. A. 2011, 108 (52), 21081–21086. [PubMed: 22167805]
33. Simonson PD; Rothenberg E; Selvin PR, Single-molecule-based super-resolution images in the presence of multiple fluorophores. Nano Lett. 2011, 11 (11), 5090–5096. [PubMed: 22003850]
34. Habuchi S; Onda S; Vacha M, Mapping the emitting sites within a single conjugated polymer molecule. Chem. Commun. 2009, (32), 4868–4870.
35. Chen L; McBranch D; Wang R; Whitten D, Surfactant-induced modification of quenching of conjugated polymer fluorescence by electron acceptors: applications for chemical sensing. Chem. Phys. Lett. 2000, 330 (1–2), 27–33.
36. Joly GD; Geiger L; Kooi SE; Swager TM, Highly effective water-soluble fluorescence quenchers of conjugated polymer thin films in aqueous environments. Macromolecules 2006, 39 (21), 7175–7177.
37. DiCesare N; Pinto MR; Schanze KS; Lakowicz JR, Saccharide detection based on the amplified fluorescence quenching of a water-soluble poly (phenylene ethynylene) by a boronic acid functionalized benzyl viologen derivative. Langmuir 2002, 18 (21), 7785–7787. [PubMed: 32165783]
38. McKinney SA; Joo C; Ha T, Analysis of single-molecule FRET trajectories using hidden Markov modeling. Biophys. J. 2006, 91 (5), 1941–1951. [PubMed: 16766620]
39. Joo C; Balci H; Ishitsuka Y; Buranachai C; Ha T, Advances in single-molecule fluorescence methods for molecular biology. Annu. Rev. Biochem. 2008, 77, 51–76. [PubMed: 18412538]
40. Vogelsang J; Adachi T; Brazard J; Bout DAV; Barbara PF, Self-assembly of highly ordered conjugated polymer aggregates with long-range energy transfer. Nat. Mater. 2011, 10 (12), 942–946. [PubMed: 21983890]

Author Manuscript Author Manuscript Author Manuscript Author Manuscript

41. Wang J; Wang D; Miller EK; Moses D; Bazan GC; Heeger AJ, Photoluminescence of water-soluble conjugated polymers: origin of enhanced quenching by charge transfer. Macromolecules 2000, 33 (14), 5153–5158.

42. Scherf U; List EJ, Semiconducting polyfluorenes—towards reliable structure–property relationships. Adv. Mater. 2002, 14 (7), 477–487.

43. Romaner L; Pogantsch A; Scandiucci de Freitas P; Scherf U; Gaal M; Zojer E; List EJ, The origin of green emission in polyfluorene-based conjugated polymers: on-chain defect fluorescence. Adv. Funct. Mater. 2003, 13 (8), 597–601.

44. Adachi T; Vogelsang J; Lupton JM, Unraveling the electronic heterogeneity of charge traps in conjugated polymers by single-molecule spectroscopy. J. Phys. Chem. Lett. 2014, 5 (3), 573–577. [PubMed: 26276611]

45. Meisel K; Vocks H; Bobbert P, Polarons in semiconducting polymers: study within an extended Holstein model. Phys. Rev. B 2005, 71 (20), 205206.

46. Bässler H, Charge transport in disordered organic photoconductors a Monte Carlo simulation study. Phys. Status Solidi B 1993, 175 (1), 15–56.

47. Gong X; Moses D; Heeger AJ; Xiao S, Excitation energy transfer from polyfluorene to fluorenone defects. Synth. Met. 2004, 141 (1–2), 17–20.

48. Im C; Bässler H; Rost H; Hörhold H, Hole transport in polyphenylenevinylene-ether under bulk photoexcitation and sensitized injection. J. Chem. Phys. 2000, 113 (9), 3802–3807.

49. Blom P; De Jong M; Vleggaar J, Electron and hole transport in poly (p-phenylene vinylene) devices. Appl. Phys. Lett. 1996, 68 (23), 3308–3310.

Author Manuscript Author Manuscript Author Manuscript Author Manuscript

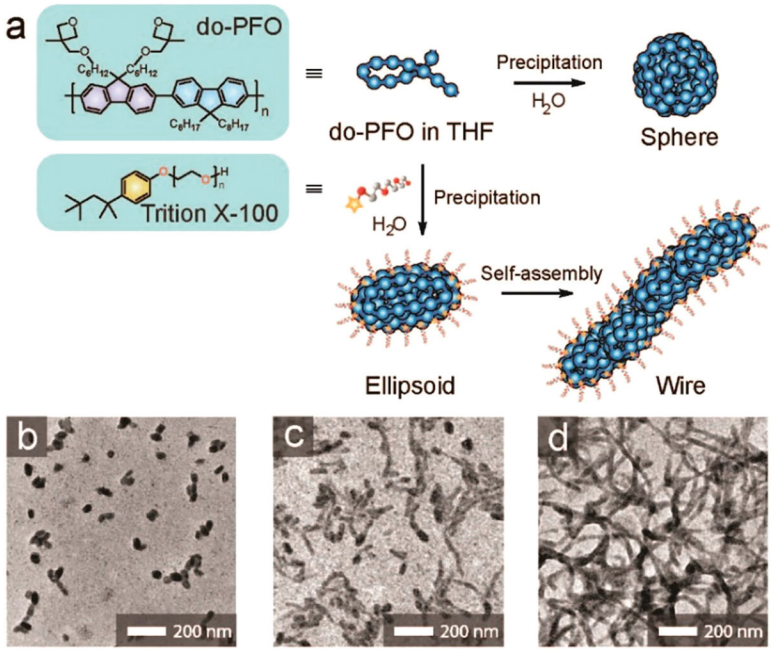

Figure. 1.

Self-assembly of various conjugated polymer nanostructures. (a) Schematic illustration of conjugated polymer nanostructures by self-assembly in a binary solvent. (b-d) Morphology evolution of conjugated polymer nanostructures by self-assembly in water in presence of 0.25 wt% Triton X-100. (b) ellipsoids, (c) mixture of ellipsoids and wires, (d) wires.

Author Manuscript Author Manuscript Author Manuscript Author Manuscript

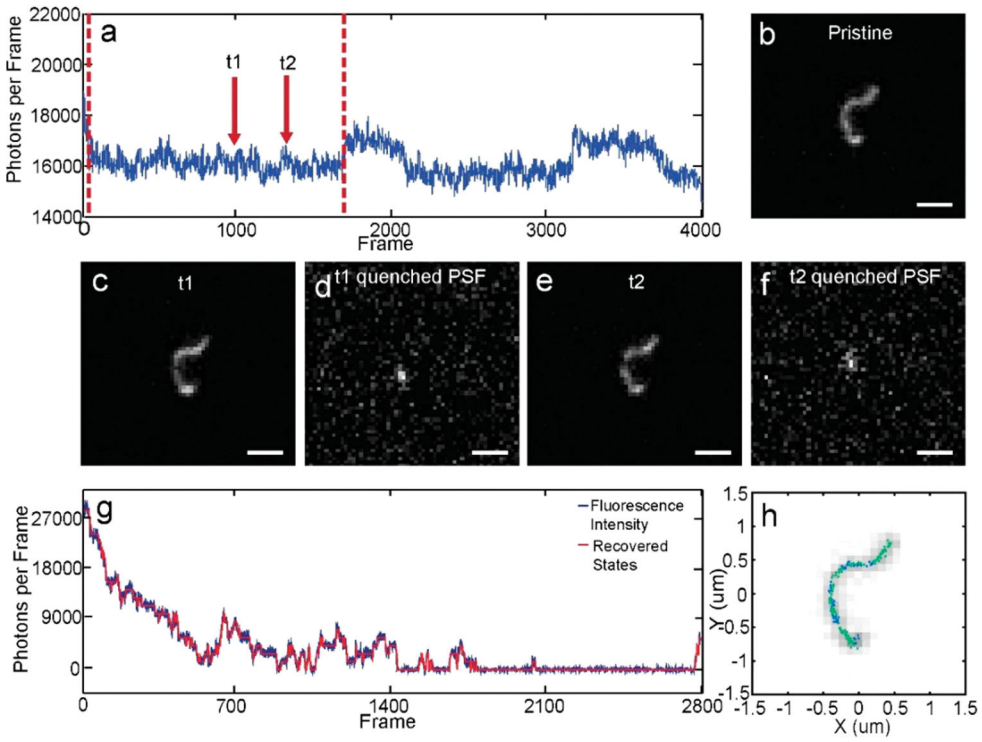

Figure. 2.

Hole polaron tracking and superresolution mapping of PFO nanowires. (a) Fluorescence intensity trajectory of a PFO nanowire, showing two-level blinking behavior. (b) A fluorescence microscopy image of the nanowire, before generation of any hole polaron. Scale bar: 1μm. (c) The fluorescence microscopy image of the nanowire after generation of a hole polaron, at t1. Scale bar: 1μm. (d) Quenched PSF, at t1. Scale bar: 1μm. (e) The fluorescence microscopy image of the nanowire after generation of a hole polaron, at t2. Scale bar: 1μm. (f) Quenched PSF, at t2. Scale bar: 1μm. (g) Fluorescence intensity trajectory of a PFO nanowire, showing binding and unbinding dynamics of MV^{2+}. Quenching and recovery steps indentified were plotted in red. (h) Superresolution image of the corresponding nanowire, overlaid with the original, diffraction-limited image. The α and β phases were plotted in dark blue and cyan, respectively.

Author Manuscript Author Manuscript Author Manuscript Author Manuscript

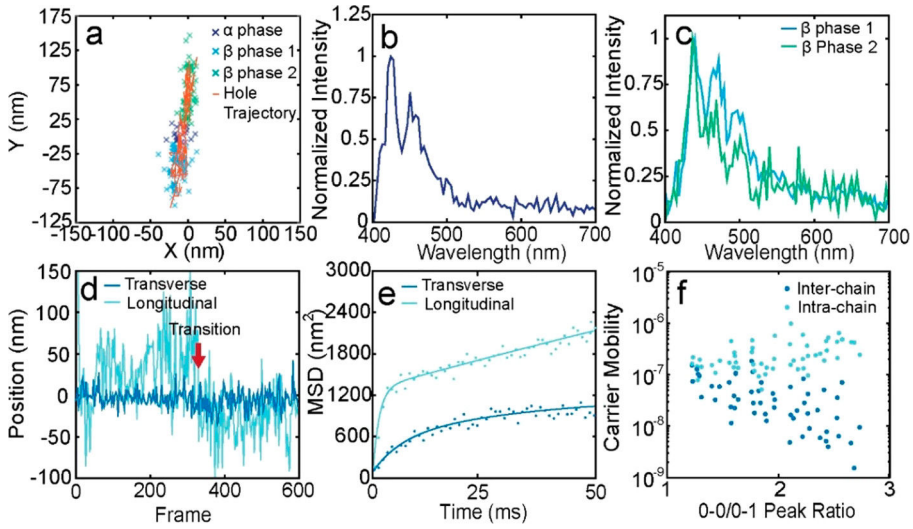

Figure. 3.

Anisotropic charge transport in PFO nanowires. (a) A hole polaron trajectory overlaid with the local superresolution spectral map, showing two β phases segmented by torsional disorder. The color of the superresolution map indicates the peak wavelength of the local emission spectrum. Binning was performed to reduce the localization uncertainty to ~5 nm. (b, c) The emission spectrum of the regions shown in panel a, indicated by different colors. (d) The corresponding longitudinal (cyan) and transverse (dark blue) single polaron motion trajectories. The red arrow indicates a transition event between the β phases. (e) Longitudinal (blue) and transverse (green) MSD of a hole polaron trajectory, both fitted to a bi-exponential confined diffusion function. $\langle x_f^2(t)\rangle = \langle x_f^2(0)\rangle + L_{f1}^2\{1-\exp(-2D_{f1}t/L_{f1}^2)\} + L_{f2}^2\{1-\exp(-2D_{f2}t/L_{f2}^2)\}$. For longitudinal transport, $D_{f1} = 4.3\times10^5$ nm^2/s, $L_{f1} = 35$ nm, $D_{f2} = 8.9\times10^3$ nm^2/s, $L_{f2} = 85$ nm. For transverse transport, $D_{f1} = 3.7\times10^4$ nm^2/s, $L_{f1} = 22$ nm, $D_{f2} = 8.3\times10^3$ nm^2/s, $L_{f2} = 25$ nm. (f) Intra-chain (cyan) and inter-chain (dark blue) hole mobilities obtained from early time MSD fitting versus 0–0/0–1 peak ratio of the local spectra.

Author Manuscript Author Manuscript Author Manuscript Author Manuscript

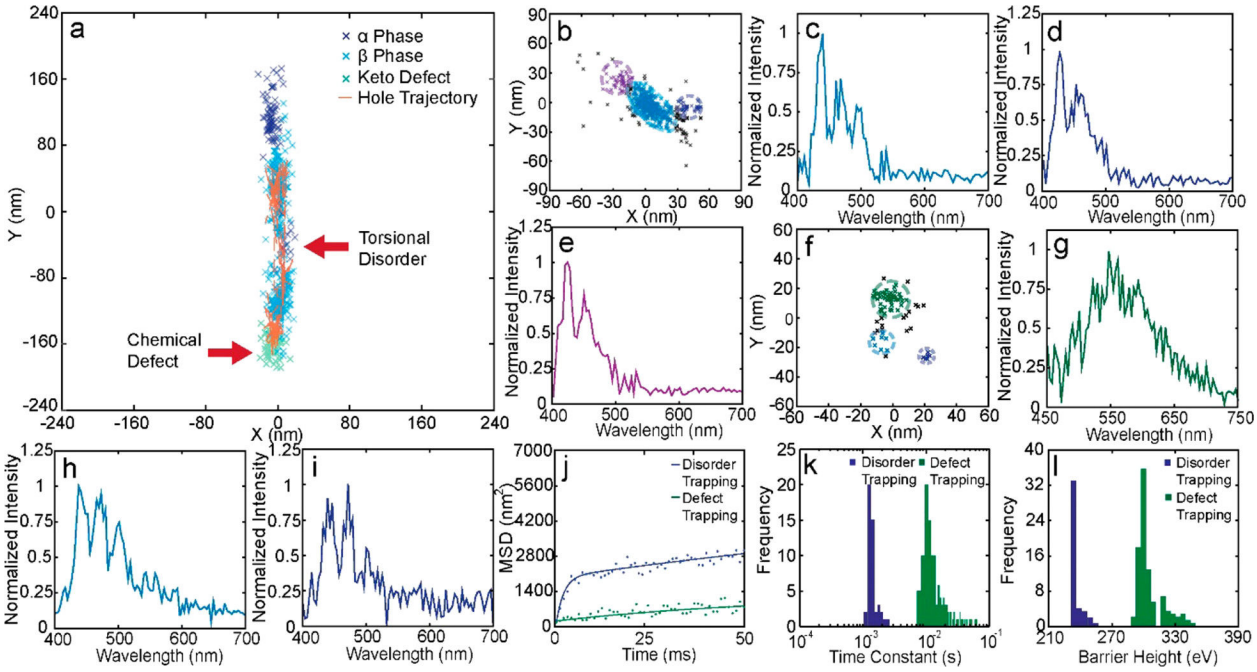

Figure. 4.

Hole polaron trapping in PFO nanowires. (a) Hole polaron trajectories overlaid with superresolution spectral map of a partially oxidized PFO nanowire. The color of the superresolution map indicates the peak wavelength of the local emission spectrum. Binning was performed to reduce the localization uncertainty to ~5 nm. (b) Localization scatter plot of a single polaron confined within a β phase between two glassy areas. (c-e) The local emission spectra of the three regions shown in panel b, indicated by different colors. (f) Localization scatter plot of a single polaron trapped around a keto defect. (g-i) The local emission spectra of the three regions shown in panel f, indicated by different colors. (j) MSDs of hole polaron trajectory segments showing disorder trapping (blue) and defect trapping behavior (green), both fitted to a bi-exponential confined diffusion function. For defect trapping, $D_{f1} = 7.2 \times 10^3$ nm^2/s, $L_{f1} = 26$ nm, $D_{f2} = 2.3 \times 10^3$ nm^2/s, $L_{f2} = 35$ nm. For disorder trapping, $D_{f1} = 6.4 \times 10^5$ nm^2/s, $L_{f1} = 43$ nm, $D_{f2} = 1.1 \times 10^4$ nm^2/s , $L_{f2} = 68$ nm. (k) Polaron escape time from glassy phase (blue) and keto defect (green). (l) Estimated depths of hole traps originated from torsional disorder (blue) and keto defects (green).